PAPER

Check for updates

Bimetallic PdPt nanoparticle-incorporated PEDOT: PSS/guar gum-blended membranes for enhanced CO_2 separation†

Nishel Saini, [a] Gaurav Pandey,[a] Ankit Sharma,[b] Kamakshi Pandey *[a,b] and Kamlendra Awasthi *[a]

To address the escalating demand for efficient CO_2 separation technologies, we introduce novel membranes utilizing natural polymer guar gum (GG), conjugate polymer (poly(3,4-ethylenedioxythiophene)-poly(styrenesulfonate)) PEDOT:PSS, and bimetallic PdPt nanoparticles. Bimetallic PdPt nanoparticles were synthesized using the wet chemical method and characterized using X-ray photoelectron spectroscopy (XPS) and transmission electron microscopy (TEM) techniques. The morphologies, chemical bonds, functional groups, and mechanical properties of the fabricated membranes were characterized using various techniques. Through meticulous fabrication and characterization, the binary blended membranes demonstrated enhanced homogeneity and smoothness in their structure, attributed to the interaction between the polymers, and superior CO_2 permeability due to the amphiphilic nature of the PEDOT:PSS polymer. Gas separation experiments performed using H_2, N_2, and CO_2 gases confirmed that the 20% PEDOT:PSS/ GG blended membranes showed the best performance with sufficient mechanical properties. Moreover, the results demonstrated an increase of 172% in CO_2 permeability and 138% in CO_2/H_2 selectivity, respectively. Furthermore, integrating bimetallic PdPt nanoparticles provided an additional 197% increase in CO_2/H_2 selectivity, owing to the unique catalytic activities of noble metal nanoparticles. The study not only underscores the transformative potential of polymer blending and noble metal engineering, but also highlights the significance of using natural polymers for sustainable environmental solutions.

1. Introduction

In recent years, the anthropogenic emission of large amounts of carbon dioxide gas has exacerbated global climate change, posing unprecedented challenges to human health, ecosystems, and socio-economic stability worldwide.[1] Along with addressing the root causes of CO_2 emissions, implementation of effective mitigation strategies has become paramount in efforts to reduce the impacts of climate change and transition towards a sustainable and resilient future.[2] In this direction, it is highly desirable to shift global energy dependency from conventional non-renewable sources to renewable sources.[3] Although various technologies have been utilized, they cannot meet global energy demands due to increasing industrialization and improved living standards of people within the present scenario. Hydrogen, with its high calorific value, pro-

vides the potential to meet this demand; however, to draw on its maximum efficiency, it needs to be purified and separated from a mixture of gases, for instance, syngas.[4] While H_2 gas can be used as a fuel, CO_2 gas should also be captured and stored for various applications, such as beverage production, food processing and preservation, fire suppression, and other medical and industrial applications.[5]

Among various techniques of gas separation, membrane technology has been found suitable due to its energy efficiency, ease of assembly, and portability, and is expected to play a significant role and continue to dominate the purification technology market.[6] The advancement in polymer membranes for gas separation provides a promising alternative to traditional energy-intensive processes and attracts a great deal of interest from researchers due to its numerous benefits, such as reduced energy consumption, lower costs, and high selectivity.[7,8] However, in the domain of membrane technology, the inherent trade-off between gas permeability and selectivity has been a longstanding challenge. To overcome this issue, considerable research efforts have been focused on various engineering strategies to enhance CO_2 separation performance,[9] such as functionalization and crosslinking strategies, incorporating various small organic and inorganic filler

aDepartment of Physics, Malaviya National Institute of Technology Jaipur, Rajasthan 302017, India. E-mail: kawasthi.phy@mnit.ac.in

bMaterials Research Centre, Malaviya National Institute of Technology, Jaipur, Rajasthan 302017, India

materials into polymer matrices to fabricate mixed-matrix membranes, and many more.[10,11] Permeation measurements have suggested that CO_2 transportation inside the membrane happens *via* the formation of intermediates such as carbamate, bicarbonate, *etc.*[12] Functionalization of polymers through various functional groups, such as the amine group, is highly preferable.[13] Furthermore, crosslinking can increase the chain mobility, reduce the fractional free volume, and enhance the size sieving ability.[14] Ali *et al.* fabricated defect-free composite membranes of highly crosslinked polyamides through interfacial polymerization of *m*-phenylenediamine (MPD) and trimesoyl chloride (TMC) that achieved H_2/CO_2 selectivity of around 50.[15] Wang *et al.* fabricated a PANI@CNT-GO/PVAm composite membrane on top of an asymmetric polysulfone support to obtain enhanced CO_2 separation performance.[16] Nigiz *et al.* fabricated GO/PDMS reverse selective membranes with enhanced CO_2/H_2 separation performance. With 0.5% GO loading, they successfully achieved a CO_2 permeability of 3970 Barrer and a CO_2/H_2 selectivity of 11.7 at 0.2 MPa pressure.[17] The fillers used in fabricating mixed-matrix membranes encompass a range of substances, including metal oxides, zeolites, MOFs, and other carbon-based materials. However, the fabrication of such membranes presents its own set of challenges, notably issues with filler compatibility, leading to filler agglomeration and consequent formation of non-uniform membrane structures with poor mechanical properties.[18] To overcome these hurdles, an appropriate selection of filler materials and their concentrations becomes essential.[19] Among other engineering methods to enhance the separation efficiency of membranes, the strategy of polymer blending by combining different polymers can be utilized to integrate the favorable aspects of polymer precursors.[9] This strategy stands out as a time-saving and cost-effective approach, yielding new membrane materials with superior properties compared to their individual polymer precursors. Polymer blending is the simplest approach for membrane fabrication, offering superior reproducibility and processability compared to alternative techniques. The fabricated membranes provide the advantages of further engineering through functionalization and incorporation of nanomaterials to enhance their separation parameters.[20]

Polymer materials can be characterized as natural and synthetic polymers based on their origin.[21] While synthetic polymers are generally non-biodegradable and can harm us in many ways, natural polymers are eco-friendly, less toxic, and readily available at low cost. Various natural polymers have been proposed for the fabrication of membranes, such as polylactic acid,[22] polysaccharides,[23] *etc.* Pal *et al.* fabricated Pd/GO/guar gum mixed-matrix membranes for enhanced CO_2 separation performance.[24] They further fabricated chitosan/guar gum composite membranes *via* crosslinking for the separation of CO_2 from H_2 and N_2 gases.[23] The utilization of natural polymers aligns with the principles of green chemistry, which advocate for the design and development of chemical products and processes that minimize or eliminate the production and use of hazardous substances.[25,26] This idea led us to utilize a natural, non-toxic, and water-soluble polymer guar gum obtained from the seeds of the *Cyamopsis tetragonolobus* plant. The polymer is made up of long chains of galactomannan polysaccharides consisting of mannose and galactose units.

Furthermore, studies have unlocked innovative possibilities with enhanced CO_2 separation performance *via* membranes fabricated from polymers having sulfonated networks due to the strong interaction between both entities.[27] Yong *et al.* prepared a sulfonated polyphenylenesulfone/polymer of intrinsic microporosity (sPPSU/PIM-1) blended membranes for CO_2 separation.[28] Such a sulfonated network in the polymer can provide up to 13% higher CO_2 uptake.[29] In this regard, PEDOT:PSS, having high chemical stability and compatible nature, provides amphiphilic properties due to the presence of abundant hydrophilic sulfonic acid groups (SO_3^-) on PSS^- and hydrophobic thiophene groups on $PEDOT^+$ chains.[30,31] Moreover, these characteristics provide enhanced possibilities for CO_2 transportation through the polymer membranes. Wang *et al.* fabricated Pebax/PEDOT:PSS blended membranes with high CO_2 permeability of 440 Barrer and CO_2/CH_4 selectivity of 28.[32] Furthermore, PEDOT:PSS provides the possibility of fine-tuning the gas separation performance through the incorporation of various gas-sensitive materials, such as noble metal nanoparticles having a special affinity towards specific gases. In our previous work, we successfully decorated noble metal Pt NPs on PEDOT:PSS membranes through the electrodeposition method with high uniformity to enhance the gas separation performance.[33] Besides single metals, bimetal nanoparticles can be very efficient in enhancing the separation parameters of the membranes due to the synergistic effects between the two metals. The bimetallic combination can enhance the chemical stability and catalytic activity of the resulting material.[34]

Through this work, we present a novel idea of blending natural polymer guar gum having excellent film-forming capabilities with conjugate polymer PEDOT:PSS having amphiphilic properties towards CO_2 gas and further engineering the blend with bimetallic PdPt nanoparticles to improve its separation capabilities. This strategic addition augments the membrane's performance in separating gases. By adopting this approach, we aim to not only investigate the gas separation characteristics of the resulting membranes, but also align our efforts with sustainability objectives, thereby promoting environmentally friendly practices in membrane technology.

2. Materials and methods

2.1. Materials required

All the chemicals were of analytical grade and utilized directly without any further modifications. For instance, palladium chloride ($PdCl_2$, 99%), dihydrogen hexachloroplatinate hexahydrate ($H_2PtCl_6 \cdot 6H_2O$, 99.9%), and L-ascorbic acid ($C_6H_8O_6$, 99%) required for the synthesis of bimetallic PdPt nanoparticles were purchased from Sigma Aldrich. Ethanol of 99% purity was purchased from Changshu Hongsheng Fine

Chemicals Co. Ltd. For the fabrication of membranes, poly (3,4-ethylenedioxythiophene)-poly(styrenesulfonate) (PEDOT: PSS, dry re-dispersible pellets) was purchased from Sigma Aldrich and guar gum was purchased from Maruti Hydrocolloids, Ahmedabad, Gujarat, India.

2.2. Synthesis of bimetallic PdPt nanoparticles

The synthesis of bimetallic PdPt nanoparticles was carried out using the following procedure as described. Initially, 133 μl of 50 mM $PdCl_2$ and an equal volume of 50 mM H_2PtCl_6 solution were added to 20 ml of deionized (DI) water. Subsequently, a few drops of 100 mM ascorbic acid were added to the resulting solution until a discernible color change was observed, indicative of reduction. The solution mixture was then aged for 20 hours to ensure the growth of the nanoparticles. Afterwards, the final reaction mixture was centrifuged at 12 000 rpm to separate the nanoparticles, which were washed four times with DI water and ethanol. The resultant bimetallic PdPt nanoparticles were then re-dispersed in 10 ml of deionized water for future use.

2.3. Fabrication of PEDOT:PSS/guar gum membranes and bimetallic PdPt nanoparticle-mixed PEDOT:PSS/guar gum membranes

The membrane fabrication process was conducted using the solution casting method, as shown in Fig. 1. At first, the polymer solution was prepared by dissolving PEDOT:PSS and guar gum polymers in de-ionized (DI) water at 40 °C. For this, specific quantities of the PEDOT:PSS polymer (1%, 5%, 10%, 15%, 20%, and 50% by weight of guar gum) were added to 25 ml of DI water and subjected to sonication for 10 minutes, followed by stirring for 1 hour at 300 rpm. A blue-colored solution was obtained. Subsequently, 189.86 mg of guar gum was added into the solution, which was then stirred for 3 hours at 300 rpm at a temperature of 40 °C. Now, a small drop of glycerol plasticizer (i.e. 0.1 wt%) was added to the solution and subjected to stirring for an additional 1 hour. The solution finally obtained was cast in a Petri dish placed over another Petri dish containing mercury and left to dry for 24 hours at a temperature of 40 °C. The role of the mercury Petri dish is to maintain a level platform to ensure uniform thickness of solution-cast membranes as mercury provides the advantage of a nearly frictionless and horizontal surface. Finally, the membranes were carefully peeled off to obtain self-standing membranes.

For the fabrication of bimetallic PdPt nanoparticle-mixed PEDOT:PSS/GG membranes (PEDOT:PSS/PdPt/GG), a 25 ml solution of bimetallic PdPt nanoparticles in DI water was utilized. The solution contains individual concentrations of Pd and Pt nanoparticles: 5.28 ppm for Pd and 16.84 ppm for Pt, as determined by the inductively coupled plasma mass spectroscopy (ICP-MS) technique. To the above solution, 20 wt% PEDOT:PSS polymer was added, followed by a series of alternating sonication and stirring cycles at 300 rpm for 1 hour, resulting in the formation of a blue-colored solution. Sequentially, guar gum and a small amount of glycerol were added along with stirring at 40 °C. The resulting solution was then subjected to the same procedure of casting in a Petri dish and drying as previously mentioned.

2.4. Characterization techniques

The synthesized bimetallic PdPt nanoparticles were characterized comprehensively to assess their structural and morphological properties along with their oxidation state. To confirm the formation of bimetallic nanoparticles and their binding states, an X-ray photoelectron spectroscopy (XPS) instrument, namely an ESCA + Omicron nanotechnology spectrometer, was utilized. The morphological characteristics of the bimetallic
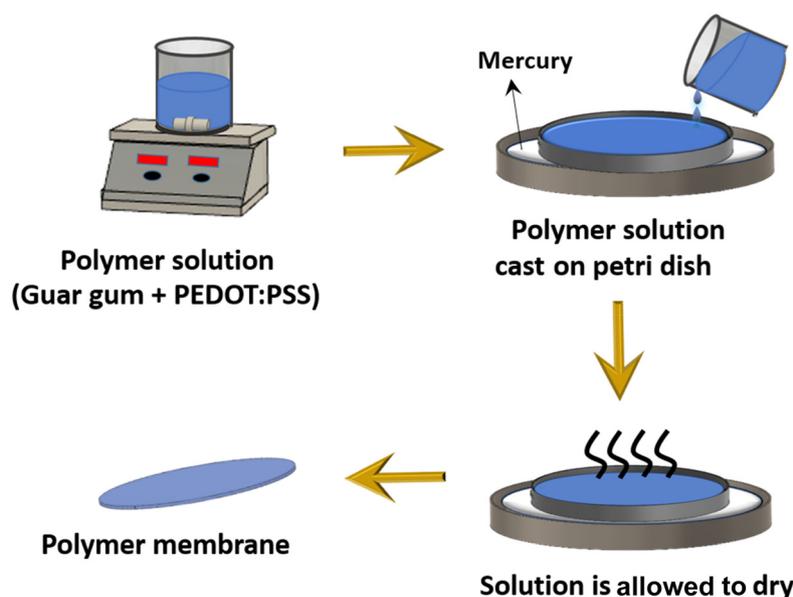

Fig. 1 Schematic of the solution-casting method utilized for the fabrication of PEDOT:PSS/GG membranes.

nanoparticles were analyzed by transmission electron microscopy (TEM) using a Tecnai G2 20 S-TWIN [FEI] instrument operating at an accelerating voltage of 200 kV. The fabricated membranes were also characterized using various techniques to gain insights into their morphology, chemical bonds, and mechanical properties. For this purpose, a field emission scanning electron microscope (FESEM), namely the Nova Nano FESEM 450, was utilized at 15 kV, a Fourier transform infrared (FTIR) spectrometer, namely a PerkinElmer Spectrum 2 set-up, was utilized in the range of 400 cm^{-1} to 4000 cm^{-1}, and a Raman spectrophotometer, namely the AIRIX STR 500, was utilized in the range of 400 cm^{-1} to 3000 cm^{-1} at an excitation wavelength of 532 nm. The mechanical properties were analyzed using a Universal testing machine, the Instron-5967, at an elongation rate of 1 mm min^{-1}. For this purpose, rectangular membrane pieces of 1.0 cm × 6.0 cm dimensions were stretched at room temperature until fractured.

2.5. Gas separation performance

The gas separation experiment of the membranes was performed using H_2, N_2, and CO_2 gases in their purest form (99.999% purity). The gas permeability values of the membranes were measured using a gas permeability setup, as explained elsewhere.[35] The formula utilized for the gas permeability calculation was derived from Fick's law; mathematically it can be given as,

$$P = \frac{Q \cdot d}{A \cdot \Delta p}$$

where the symbols have their usual meanings: P is the permeability of the gas in Barrer (1 Barrer = 10^{-10} cm^3 (STP) cm (cm^2 s cmHg)$^{-1}$), d is the membrane thickness, Q represents

the mass flow rate, A is the effective cross-sectional area of the membrane, and Δp is the pressure difference across the two sides of the membrane. All the gas separation experiments were carried out at room temperature and under a pressure of 10 psi. The room temperature conditions were chosen for the experiments due to the temperature constraints of the polymers as their mechanical and physical properties may deteriorate with increasing temperature. Furthermore, the effective area of the membranes used for the gas separation experiment is 13.19 cm^2. The gas selectivity was calculated from gas permeability values by using the following relationship,

$$S = \frac{P_A}{P_B}$$

where P_A and P_B are the gas permeabilities of the two gases, respectively.

3. Results and discussion

3.1. Characterization of bimetallic PdPt nanoparticles

Fig. 2(a) shows the typical survey spectrum of the material in the range of 0–1000 eV, revealing the characteristic peaks corresponding to Pt, Pd, C, and O in the material. Fig. 2(b) and (c) exhibit the high-resolution spectra of the material, showing the electron binding energies of the palladium and platinum elements in the material, respectively. Fig. 2(b) shows two distinct peaks of palladium metal, *i.e.* Pd 3d$_{5/2}$ at 340.3 eV and Pd 3d$_{3/2}$ at 335.2 eV, representing the Pd^0 states of palladium. Furthermore, the figure also shows that these peaks are overlapped with the peak of platinum (Pt 4d$_{3/2}$). Similar Pd and Pt peaks overlapping in the XPS spectrum have also been reported earlier.[36] The higher intensity of the Pt
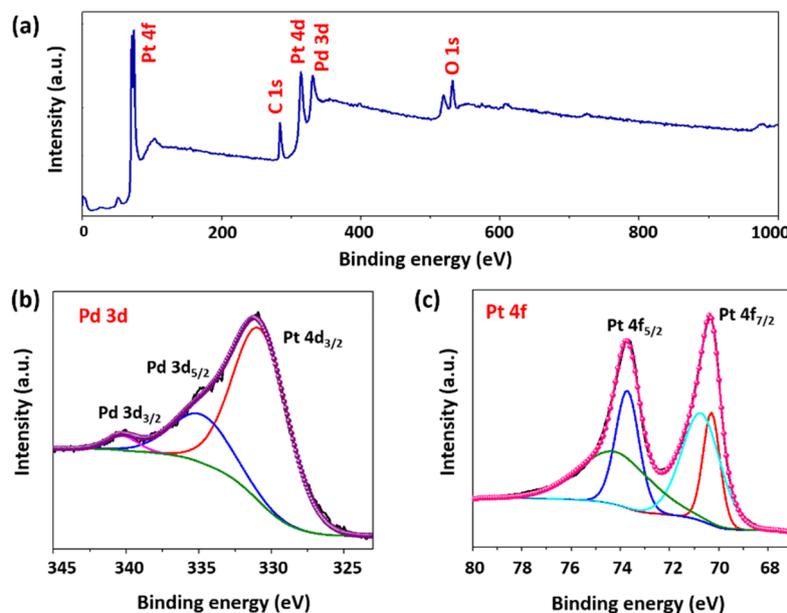

Fig. 2 XPS survey scan spectra of (a) the bimetallic PdPt nanoparticles, (b) Pd 3d, and (c) Pt 4f.

peak provides the possibility of either a higher content of Pt in the material or the presence of Pt element on the surface with Pd in the bulk.[37,38] This discrepancy in the peak intensity is resolved through the bulk-sensitive inductively coupled plasma mass spectroscopy (ICP-MS) technique, which confirmed a lower concentration of Pd (5.28 ppm) and a higher concentration of Pt (16.84 ppm) in the bimetallic PdPt nanoparticle solution prepared in DI water. In Fig. 2(c), each Pt 4f line is deconvoluted into two components associated with two distinct oxidation states of platinum, as indicated by their electron binding energies corresponding to Pt $4f_{5/2}$ and Pt $4f_{7/2}$.[39] Among these, the peaks at higher binding energies, *i.e.* 74.4 eV (Pt $4f_{5/2}$) and 70.8 eV (Pt $4f_{7/2}$), are associated with metallic Pt, *i.e.* Pt^0,[40] while the peaks at lower binding energies, 73.7 eV (Pt $4f_{5/2}$) and 70.3 eV (Pt $4f_{7/2}$), are associated with the Pt^{II} states of platinum. The XPS result confirms the lower amount of Pd and the higher amount of Pt at the material's surface. The survey spectra were utilized to obtain the atomic percentage of the material and the results revealed that Pd constitutes approximately 20%, while Pt accounted for around 60% of the surface composition. The remaining signal was attributed to other elements such as C and O, which contribute around 10% and 9%, respectively. Also, the peaks corresponding to the palladium and platinum bimetallic systems have shifted to lower binding energy values due to the charge transfer and electronic disturbances created by a change in the chemical environment as a result of alloy formation. Such interactions enhance the catalytic activity and durability of the material.[41]

Fig. 3(a) depicts the TEM image of bimetallic nanoparticles, and the results revealed the formation of well-defined spherical nanoparticles with an average particle size of approximately 67 nm. The majority of particles lie in the range of 60–70 nm, as shown in the histogram representing particle size distribution, and were calculated using the Gaussian fitting methodology (see Fig. 3(b)). The high-resolution transmission electron microscopy (HRTEM) and selected area electron diffraction (SAED) patterns, illustrated in Fig. 3(c) and (d), respectively, were utilized to acquire crucial details regarding the crystallographic structure and orientation of the nanoparticles. Remarkably, HRTEM analysis revealed an interplanar spacing of 0.229 nm, indicative of the (111) planes of the face-centered cubic (FCC) structure within the synthesized nanoparticles.[42] Additionally, the diffraction spot pattern observed *via* SAED exhibited circular bright rings corresponding to the (111), (200), and (220) planes of the polycrystalline nanoparticles. These findings are consistent with the existing literature,[34] underscoring the validity and significance of our results within the broader scientific context.

In addition to various characterization methods of bimetallic nanoparticles, the membranes were also characterized comprehensively to gain a thorough understanding of various properties, which is crucial for correlating their structural attributes with performance metrics.
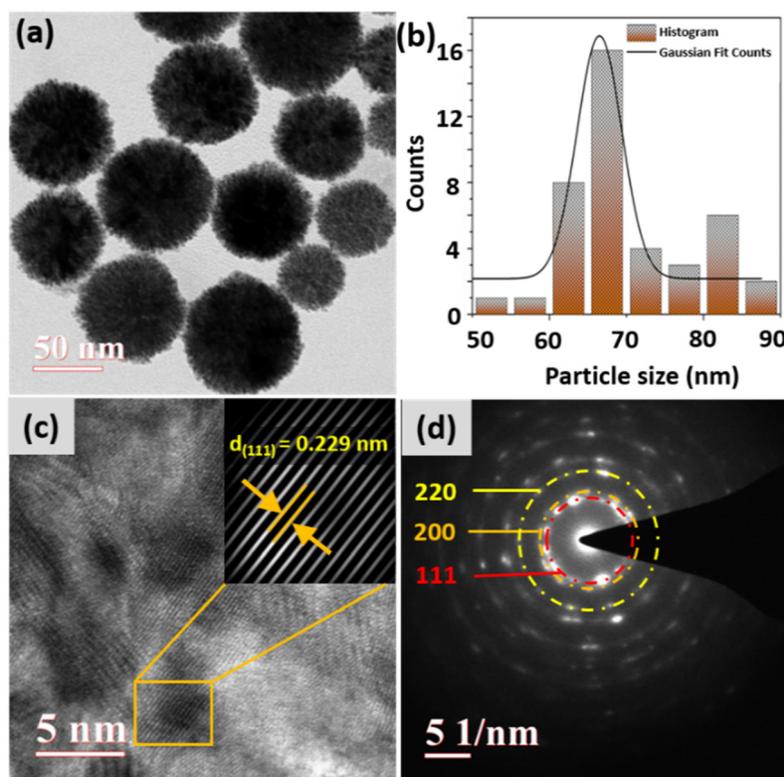
Fig. 3 (a) TEM images, (b) histogram representing the average particle size, (c) HRTEM images, and (d) SAED pattern of the bimetallic PdPt nanoparticles.

3.2. Fourier transform infrared (FTIR) spectroscopy

Following the fabrication process, the membranes were subjected to characterization using various techniques to study their chemical and morphological features. The chemical interactions within the pure polymers and the synthesized blends (5%, 10%, and 20% PEDOT:PSS/GG) were analyzed using the FTIR spectroscopy technique, and the corresponding spectrum is shown in Fig. 4. Upon examining the spectrum, it can be observed that all the characteristic peaks corresponding to both the guar gum (GG) and PEDOT:PSS materials are present in the spectrum, as also confirmed through the already reported literature.[33,43] Notably, the peaks at 811 cm^{-1} and 870 cm^{-1} signify the C–H stretching and bending vibrations of the aromatic ring, while the peaks at 1015 cm^{-1}, 1062 cm^{-1}, and 1144 cm^{-1} correspond to the vibrations associated with the ester (–C–O–C–) group of the guar gum material.[24] Table S1 (ESI†) presents the detailed peak assignments for the guar gum material, while the peak positions and their bond assignments corresponding to the PEDOT:PSS material are outlined in Table S2 (ESI†). The analysis of the PEDOT:PSS spectrum revealed that the peaks at 854 cm^{-1} and 1008 cm^{-1} represent the vibrations corresponding to the C–S–C bond in the thiophene ring of PEDOT. Similarly, the peaks at 1125 cm^{-1} and 1256 cm^{-1} correspond to the asymmetric and symmetric stretching of the ester (–C–O–C–) group (see Table S2†).[44,45] Fig. 4 shows the emergence of some new peaks at positions around 1213 cm^{-1} and 1370 cm^{-1} in the case of the blended membrane, which are the characteristic peaks of the PEDOT:PSS material, with slight shifting towards lower wavenumber, *i.e.* redshift. Moreover, the intensities of these peaks increased on increasing the content of the PEDOT:PSS material, while certain peaks corresponding to the guar gum material diminished after adding PEDOT:PSS, which is a result of the interaction between both the polymers.[46] The observed peak shifts are attributed to the conformational changes due to the blending of the polymers, resulting in changes in bond lengths and the chemical environment.[32]

The findings from FTIR spectroscopy clearly explain the composition and interaction dynamics within the polymers. The interaction within the polymers is also evident in the prepared polymer solutions. The pure GG solution exhibited high viscosity, likely attributable to the significant amount of hydrogen bonding within the polysaccharide chain structure. However, upon mixing PEDOT:PSS with GG, the viscosity of the solution is reduced, which is associated with the ability of PEDOT chains to disrupt the intermolecular H-bonding within the polysaccharide chains of guar gum. Similar observations have been reported in previous studies, which confirm the validity of these findings.[47] FTIR measurements were also conducted for the 20% PEDOT:PSS/PdPt/GG composite membranes before and after testing their hydrogen separation performance and the resulting spectrum is shown in Fig. S1 (ESI†). The findings confirm slight changes in the peak intensity and peak broadening, particularly, in the fingerprint region (500 cm^{-1} to 1500 cm^{-1}) and the O–H stretching region (3300 cm^{-1} to 3500 cm^{-1}). For instance, the intensity of the broad peak at around 3300 cm^{-1} reduces and the peak becomes more defined. Such changes in the peak intensity and sharpening of the peak confirm the interaction of H₂ with the hydroxyl group or an effect on the hydrogen bonding network within the polymer matrix, impacting the polymer matrix.[48] Also, the peak at around 596 cm^{-1} corresponding to metal–sulfur (M–S) and metal–oxygen (M–O) vibrations disappeared after the samples were treated in the presence of hydrogen, indicating the change in the environment associated with bimetallic PdPt nanoparticles.[49]

3.3. Raman spectroscopy

Raman characterization of the material was carried out to unveil numerous distinct vibrational bands that are indicative
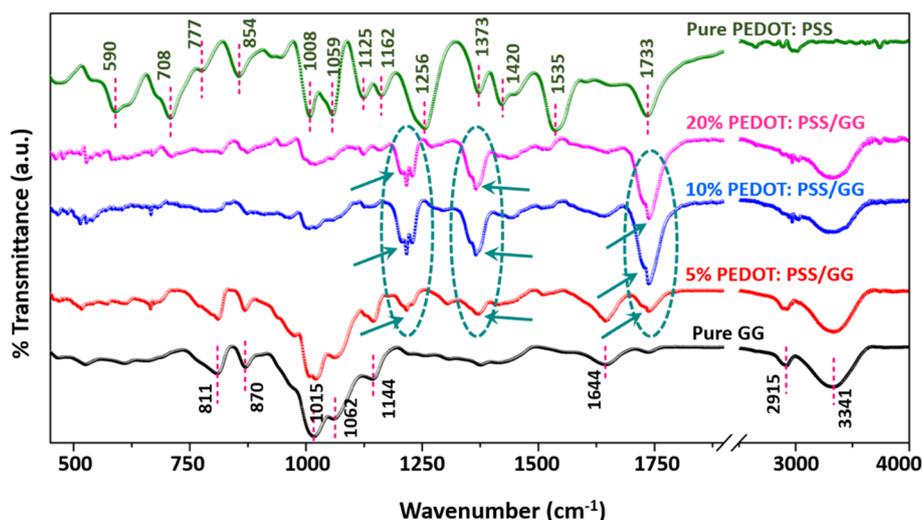

Fig. 4 FTIR spectra of the pure GG, pure PEDOT:PSS, and PEDOT:PSS/GG membranes.

of the particular molecular vibrations and functional groups within the sample. The Raman spectra of the pure PEDOT:PSS material, pure GG, and the 20 wt% PEDOT:PSS/GG composite membrane in the range from 500 cm^{-1} to 3000 cm^{-1} are presented in Fig. 5. The peaks match perfectly with the already reported data for the PEDOT:PSS and GG materials.[50] For instance, in the PEDOT:PSS material, the peaks at 694 cm^{-1}, 872 cm^{-1}, 984 cm^{-1}, and 1100 cm^{-1} correspond to the different vibrational modes of PSS, *i.e.* symmetric S–S–C deformation, bending vibrations of the C–H group and C–O–C

deformation, respectively. The peaks corresponding to PEDOT vibrational modes are obtained at 1260 cm^{-1}, 1361 cm^{-1}, 1425 cm^{-1}, 1505 cm^{-1}, and 1548 cm^{-1}, respectively.[50,51] In the Raman spectrum of the guar gum polymer, the major peaks observed in the range from 800 cm^{-1} to 950 cm^{-1} correspond to its anomeric skeletal configuration, while the peaks at around 1097 cm^{-1} and 1112 cm^{-1} are due to C–O–C symmetric and asymmetric vibrations, and the peak at 1269 cm^{-1} is due to the CH_2OH group.[52] Furthermore, the peaks at 1342 cm^{-1}, 1386 cm^{-1}, 1408 cm^{-1}, and 2885 cm^{-1} are due to the C–OH bending, in-plane C–H bending, and C–H stretching vibrations, respectively.[53] Again, in the Raman spectrum of the 20 wt% PEDOT:PSS/GG composite membrane, as shown in Fig. 5, all the peaks are mainly analogous with those of pure GG with a slight blue shift for some of the peaks, which can be due to the result of conformational changes due to blending of polymers, resulting in an alteration in the vibrational modes of the polymer.[54,55]
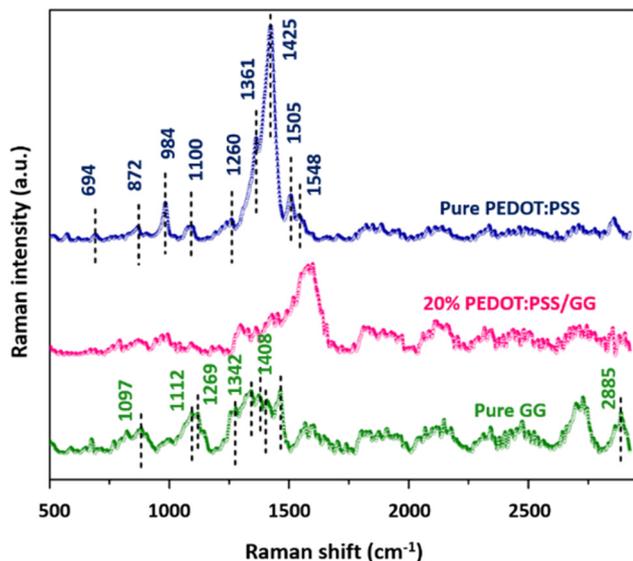
3.4. Field emission scanning electron microscopy (FESEM)

Fig. 6 shows the field emission scanning electron microscopy (FESEM) images of the pure GG, 5% PEDOT:PSS/GG, 20% PEDOT:PSS/GG, and bimetallic PdPt nanoparticle-mixed 20% PEDOT:PSS/GG membranes. Analysis of these images reveals a remarkably consistent and smooth morphology, which confirms uniform distribution of polymer constituents without apparent surface defects and irregularities. Hence, there is successful blending between both polymers at the molecular level up to some concentration values. Such a uniformly blended structure using the PEDOT:PSS polymer has already been reported earlier.[32] Guar gum contains hydroxyl (–OH) groups in its structure, which can participate in hydrogen bonding

Fig. 5 Raman spectra of the pure GG, pure PEDOT:PSS, and 20% PEDOT:PSS/GG membranes.
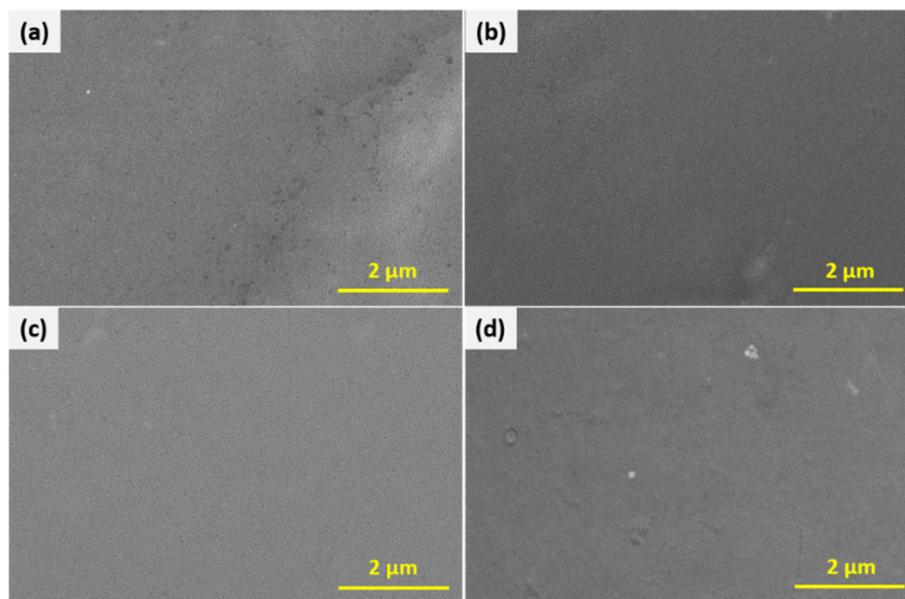

Fig. 6 Top surface FESEM images of the (a) pure GG, (b) 5% PEDOT:PSS/GG, (c) 20% PEDOT:PSS/GG, and (d) 20% PEDOT:PSS/PdPt/GG composite membranes.

interactions with various functional groups present in PEDOT: PSS, such as sulfonate groups ($-SO_3^-$) in PSS. These hydrogen bonds facilitate adhesion and interaction between the two polymers, resulting in membranes with no voids and absence of defects. Such a smooth morphology with minimum defects, cracks, and pinholes is crucial for achieving enhanced separation performance and gas selectivity.[56] The membranes procured by blending the two polymers were highly uniform with impressive flexibility up to a certain amount of loading. The top surface image in Fig. 6(d) shows some roughness in the structure and some white spots, confirming the presence of the bimetallic PdPt nanoparticles. Fig. S2 (ESI†) shows the photographs of the front view of these membranes and Fig. S3 (ESI†) displays their folded view, demonstrating their flexible nature through bending. However, the folded image of the 50% PEDOT:PSS/GG membrane is not shown as it fractured when folded, confirming its high brittleness, which is also validated through its lower tensile strength and poor mechanical properties, as shown in the next section. At higher concentrations of the PEDOT:PSS polymer, the membrane structure becomes more rigid and brittle, as compared to the flexible and elastic nature of pure guar gum due to the presence of π–π stacking interactions between the conjugate polymer chains. These results are confirmed through the reduction in the mechanical properties of the membranes as discussed in the upcoming section of this work. Fig. 7 shows the cross-sectional FESEM images of the pure GG, 5% PEDOT:PSS/GG, and 20% PEDOT:PSS/PdPt/GG composite membranes, respectively, confirming that the thicknesses of the membranes ranged from around 25 μm to 33 μm. The thickness of the membrane sample is greatest at higher PEDOT:PSS material content due to the combined effect of particle incorporation and polymer interaction, leading to structural reinforcement. Furthermore,

the cross-sectional images confirm the dense and almost uniform morphology of all the samples. The maximum uniformity and smooth structure at higher loading of the PEDOT: PSS polymer confirms the effective distribution of both PEDOT:PSS and PdPt within the guar gum matrix.

The energy-dispersive X-ray spectroscopy (EDS) mapping of S, C, O, Pd, and Pt was performed for the bimetallic PdPt nanoparticle-mixed 20% PEDOT:PSS/GG composite membranes. The resulting top-surface images, as shown in Fig. 8, and cross-sectional images, as shown in Fig. S4 (ESI†) unequivocally confirm the presence and homogeneous attachment of the bimetallic PdPt nanoparticles across the membrane surface and its bulk.

3.5. Mechanical properties

Besides good interaction between both polymers and a lack of visible surface defects, as discussed above, the addition of PEDOT:PSS to the guar gum altered the internal structure and mechanical properties of the composite membranes, which can be due to the inherent brittle nature of the PEDOT:PSS material.[57,58] In general, membranes having homogeneous structures, without any cracks and pinholes, can resist mechanical stress, while defects act as stress concentrators, leading to mechanical failure of the membranes even at lower stress levels; conversely, the smoother surface morphology can be linked to better polymer interaction and better dispersion of nanomaterials, which contribute to higher mechanical strength. Fig. 9 shows the stress–strain (%) plot for the composite membranes of PEDOT:PSS/guar gum. From the figure, it is evident that the pure guar gum showed a maximum tensile strength of 27.14 MPa with an extension of 0.76 mm, representing its plastic behaviour. The addition of the PEDOT:PSS polymer to the guar gum resulted in the reduction of mechani-
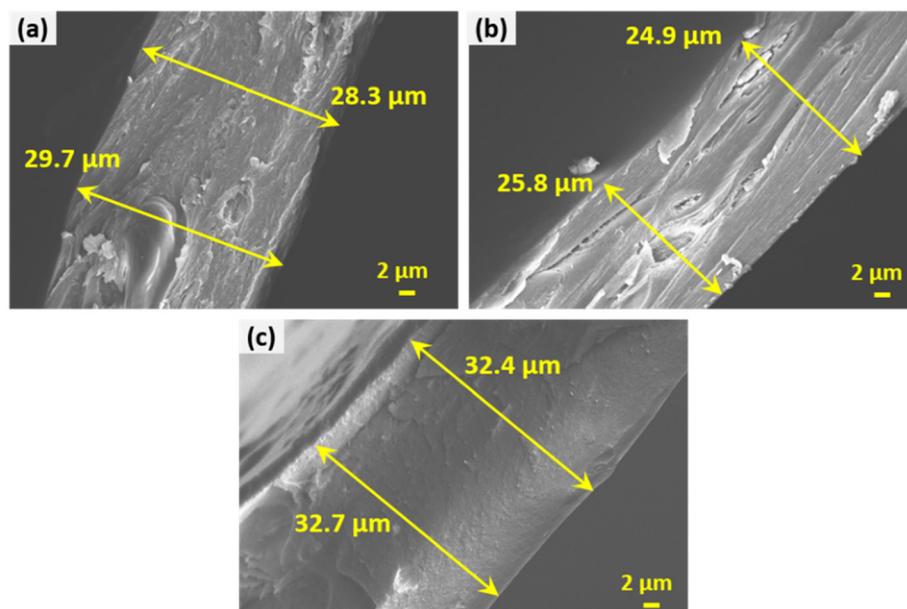

Fig. 7 Cross-sectional FESEM images of the (a) pure GG, (b) 5% PEDOT:PSS/GG, and (c) 20% PEDOT:PSS/PdPt/GG composite membranes.
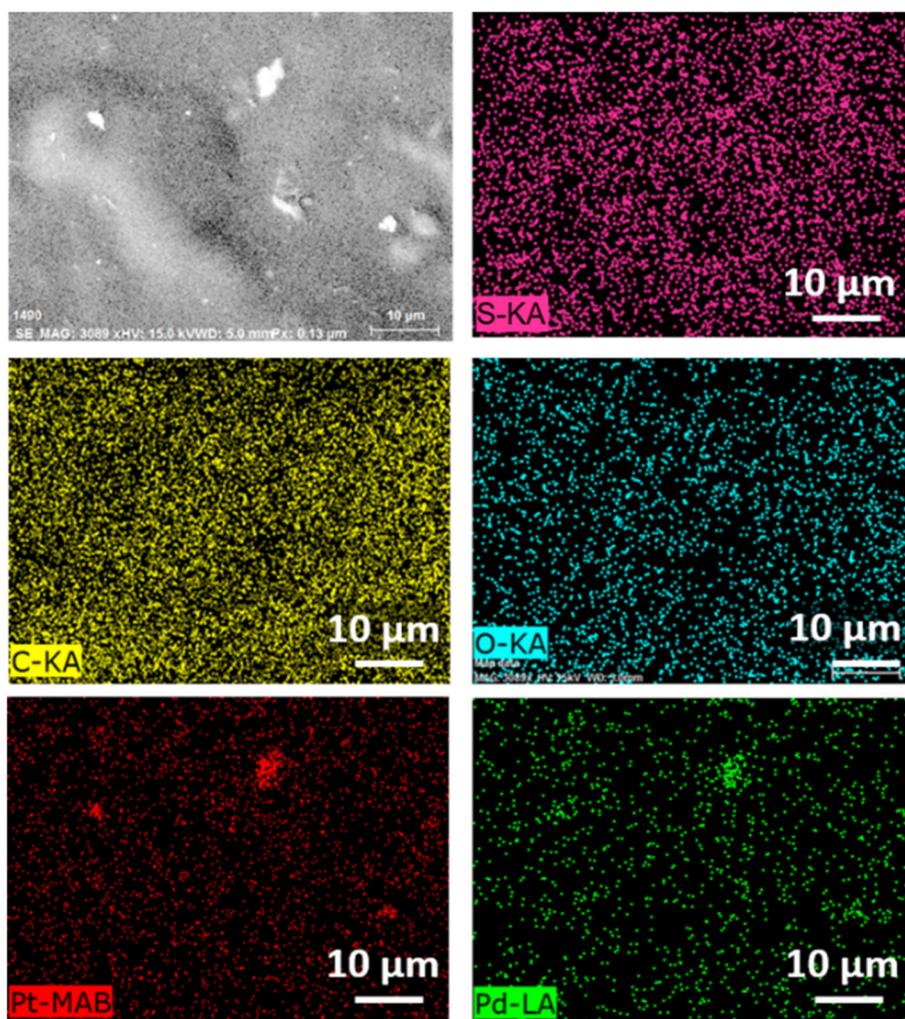
Fig. 8 Top-surface EDS mapping images of S, C, O, Pt, and Pd elements in the 20% PEDOT:PSS/PdPt/GG composite membranes.
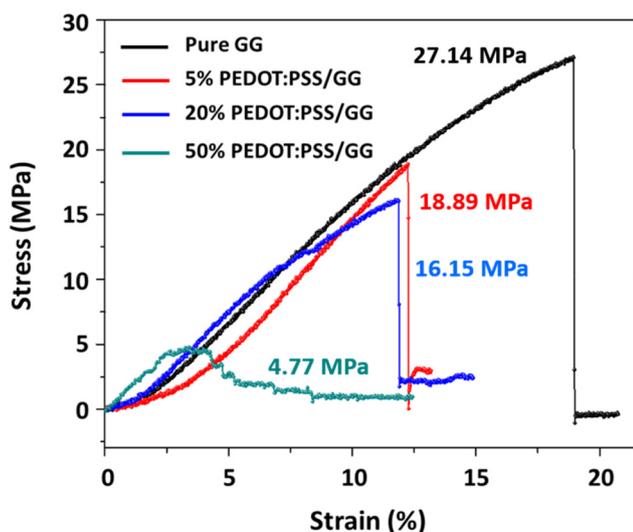

Fig. 9 Stress–strain curves of the PEDOT:PSS/GG composite membranes.

cal strength of the composite membranes. The 5% PEDOT:PSS/GG membrane showed a reduced tensile strength of 18.89 MPa and 20% PEDOT:PSS/GG showed a further reduction to 16.15 MPa, with a corresponding decrease in flexibility. This decrease confirms that the incorporation of PEDOT:PSS has introduced some structural modifications within the polymer matrix due to the disruption of intermolecular hydrogen bonding within the polysaccharide chains of guar gum, as also confirmed from the FTIR results in the previous section. The 50% PEDOT:PSS/GG membrane showed a significant reduction in its tensile strength value to only 4.77 MPa, demonstrating the concentration-dependent effect. These membranes were brittle and not able to withstand the applied pressure for a long time due to their brittleness. The high concentration of PEDOT:PSS leads to micro-crack formation during elongation, resulting in premature failure of the membrane under pressure. In general, the PEDOT:PSS polymer contains π–π stacking interactions, which make it a more ordered and stronger structure with restricted mobility of the polymer chains, leading to a more rigid and brittle membrane as com-

pared to the pure guar gum. Hence, even with the uniform and smooth structure of the membranes as shown in the FESEM images of Fig. 6, they show poor mechanical properties on increasing the content of the PEDOT:PSS polymer.

4. Gas separation performance

The H_2, N_2, and CO_2 gases in their purest form were used to carry out the gas permeability measurements in this work. Fig. 10 shows the gas separation performance of the membranes. From the graph, it can be easily observed that the membranes exhibit their highest permeability value towards H_2 gas among the tested gases due to its the smallest kinetic diameter. However, on increasing the content of PEDOT:PSS in

the membrane, the CO_2 permeability and selectivity values increase up to 20% PEDOT:PSS loading, after which the values became saturated while the permeability of the remaining gas did not change much. The increase in CO_2 permeability value is due to the presence of high CO_2-philic and non-CO_2-philic networks within the structure of PEDOT:PSS.[32,46] The basic interaction mechanism between the PEDOT group and the CO_2 molecules can be both chemisorption and physisorption. However, chemisorption requires high energy to cross the barrier, which is not feasible at room temperature. The energy required for the physisorption reaction is much less, indicating the possibility of a strong interaction between the material and the gas molecules at room temperature. Specifically, the presence of π-conjugation in the backbone of the conducting polymer PEDOT:PSS can increase CO_2 adsorption due to the
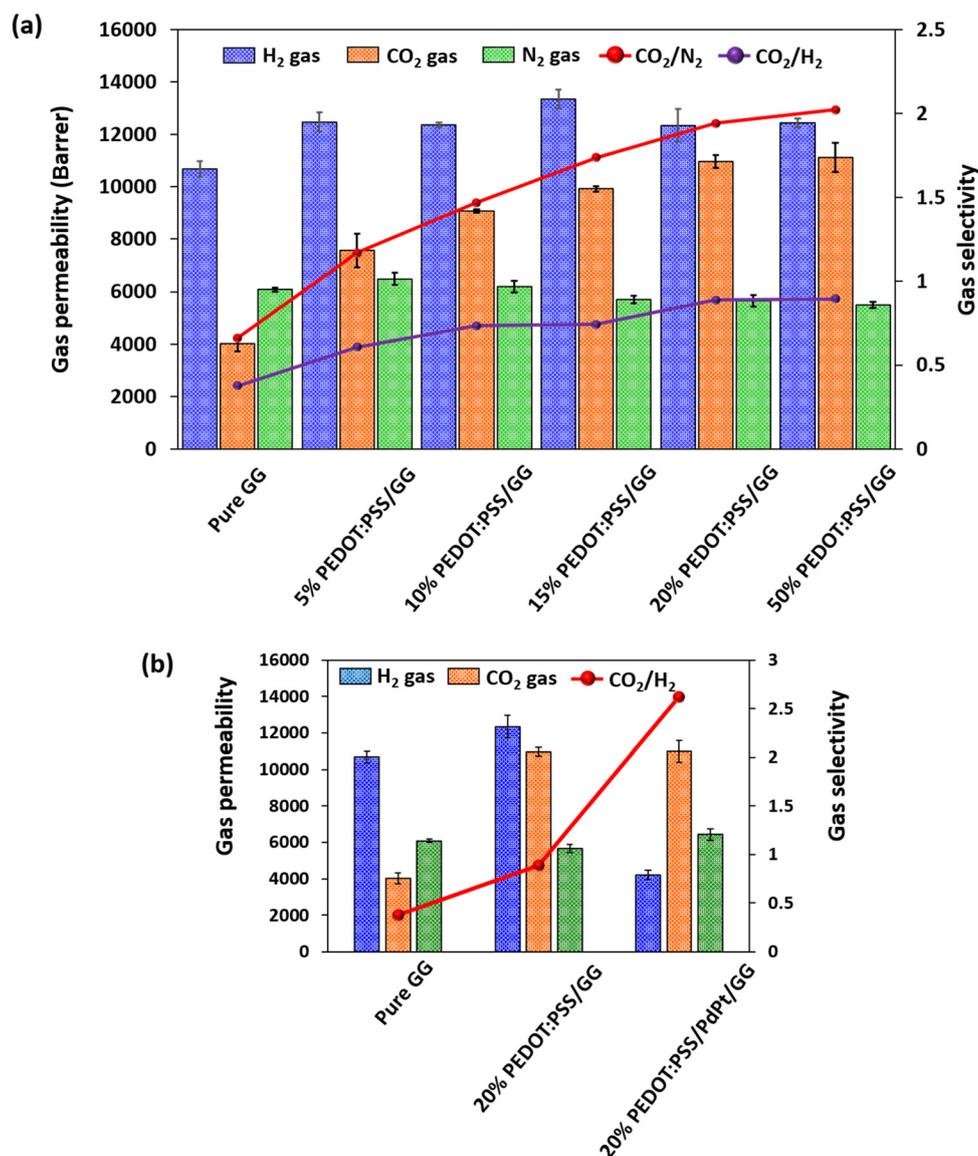

Fig. 10 Gas separation performances of the PEDOT:PSS/guar gum composite membranes at 10 psi pressure (a) at different wt% values of guar gum and (b) with bimetallic PdPt nanoparticles.

π–π interaction of delocalized π-conjugated electrons with CO_2 molecules. The benzene rings and sulfonic acid groups on the PSS chain can strongly bind CO_2 molecules due to the quadrupole–π interactions, hydrogen bonding, and electrostatic interactions favouring its transportation. The observed trends highlight that while PEDOT:PSS enhances gas separation performance due to its increased CO_2 selectivity, its higher concentration compromises the mechanical integrity of the membranes. Since the 20% PEDOT:PSS/GG composite membrane showed a maximum CO_2 permeability value of 10 970 Barrer and CO_2/H_2 and CO_2/N_2 selectivity values of 0.88 and 1.94, which are increases of around 172%, 138%, and 193%, respectively, while also exhibiting sufficient mechanical strength as compared to membranes at higher loading of PEDOT:PSS (as also confirmed through the stress–strain plot in Fig. 9), the 20% PEDOT:PSS/GG composite membrane was further incorporated with bimetallic PdPt nanoparticles having better adsorption properties towards H_2 gas due to their higher surface to volume ratio, stronger H_2 affinity and synergistic effect between both the noble metal nanoparticles. On adding the bimetallic PdPt nanoparticles, the H_2 permeability was reduced from 12 347 Barrer to 4200 Barrer,

which is a decrease of almost 66%, while maintaining the gas permeability values of the remaining two gases at almost the same level, while the CO_2 selectivity was increased from 0.88 to 2.62, which is an increase of almost 197%, as shown in Fig. 10(b). To further demonstrate the stability and durability of the 20% PEDOT:PSS/GG and 20% PEDOT:PSS/PdPt/GG composite membranes, we conducted the gas separation experiment over a period of 24 hours and observed a consistent performance throughout the experiment. Fig. S5 (ESI†) presents the results of the gas permeability and selectivity data for the experiment conducted over 24 hours using CO_2 and H_2 gases.

The gas separation performance of the membranes was also compared with the data reported in the literature and the Robeson upper bound, as shown in Fig. 11. From the figure, it can be seen that although the blending of PEDOT:PSS and guar gum has significantly improved the gas separation data of the membranes, the performance did not surpass the Robeson upper bound 2008, although it successfully crossed the upper bound 1991 for both CO_2/N_2 and CO_2/H_2 gas pairs. Furthermore, the incorporation of bimetallic PdPt nanoparticles efficiently enhanced the CO_2/H_2 selectivity values due to their higher affinity and absorbing capacity towards H_2
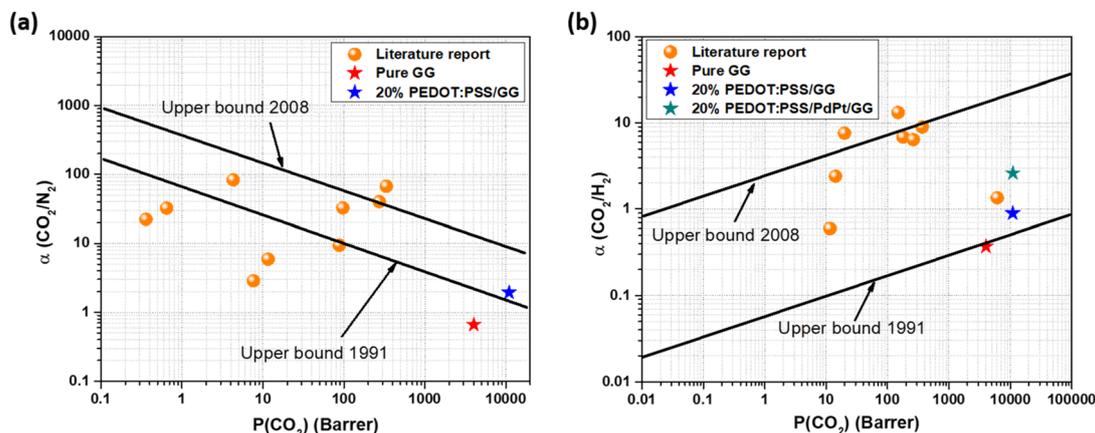

Fig. 11 Comparative assessment of gas separation performance against the Robeson upper bound and previously published work for (a) CO_2/N_2 and (b) CO_2/H_2 separation.

Table 1 Representation of the data from the previously reported literature used for comparison with the Robeson upper bound plots

Membrane material	Nature of membrane	CO_2 gas permeability (Barrer)	CO_2/H_2	CO_2/N_2	Ref.
P3HET/P3AcET	MMM	336	—	67.2	59
PPy/Pebax-1657	MMM	274	—	40	60
PPy/PC	MMM	11.6	0.595	5.9	61
Sandwich-like PANI/EVA	Supported	97.5	—	32.5	62
PANI/aniline/PSF	Supported	4.3	—	83	63
Polyimide	Self-supported	1242	1.44	—	64
Pebax and PVA	Polymer blending	19.98	7.6	—	65
Jeffamine ED-2003 and GOTMS	MMM (polymer crosslinking)	367	8.95	—	66
PEO-600 and PEO-526	MMM (polymer crosslinking)	180	6.84	—	67
MWCNT/Pebax 1657	MMM CNT/polymer	262	6.40	—	68
TDI/MWCNT/Pebax 1657	MMM CNT/polymer	14.28	2.4	—	68
ZIF-67/PIM	MOF/polymer	6118	1.35	—	69
20% PEDOT:PSS/GG	Polymer blending	10 970	0.88	—	This work
20% PEDOT:PSS/PdPt/GG	Polymer blending	11 000	2.62	—	This work

molecules. Hence, the blending of the amphiphilic polymer PEDOT:PSS and guar gum has proved to be efficient in improving the CO_2 separation performance of the membranes with sufficient mechanical properties, and the material combination has proved to be good and effective in the direction of usage of novel and natural polymer in the fabrication of gas separation membranes. Table 1 provides a comparison of the results from the present work with those of previously reported data using various types of membranes, highlighting the performance of the present membranes.

5. Conclusion

In conclusion, the fabrication of polymer-blended membranes utilizing guar gum and PEDOT:PSS materials has shown promising results for gas separation applications by imparting complementary properties to the resulting membranes. While the guar gum provided good film-forming capabilities, along with biocompatibility and mechanical strength, the PEDOT: PSS polymer improved the separation performance of the membranes towards CO_2 gas due to the co-existence of both CO_2-philic and non-CO_2-philic groups, resulting in faster CO_2 transport. Our findings indicate that on increasing the content of PEDOT:PSS in the membrane, the CO_2 permeability increased from 4024 Barrer to 11 001 Barrer, while the H_2 and N_2 permeability values were not affected much, confirming the potential of tailoring the gas transport properties by adjusting the composition of the polymer blend. Furthermore, it was observed that the blended membranes showed smoother and uniform morphologies with minimal imperfections and defects, and significant molecular-level compatibility between both the polymers, which are crucial for ensuring the integrity and performance of the membranes. However, beyond a certain concentration of PEDOT:PSS, the mechanical properties of the membranes deteriorate due to the rigid and brittle nature of the PEDOT:PSS polymer. However, a balance is achieved at 20% PEDOT:PSS concentration that offers the optimal compromise between mechanical strength and separation performance.

Overall, the study underscores the efficacy of blending a conjugate polymer with a natural polymer in fabricating efficient gas separation membranes with good separation performance. Furthermore, the successful integration of bi-metallic nanoparticles highlights the potential of tuning membrane performance for specific gases. Moreover, these findings contribute to the ongoing development of advanced materials in membrane technology for gas separation applications. This study represents a significant advancement in our quest for exploiting natural polymer for gas separation applications using the polymer blending strategy by combining it with the high-performing PEDOT:PSS polymer having an active site towards CO_2 molecules. The integration of bimetallic PdPt nanoparticles provided an additional advantage. The outcomes presented in this study provide groundwork to further explore the membranes under different operational parameters, such as the effect of pressure, gas mixture conditions *etc.*, which are essential for translating these membranes into real and practical applications.

Abbreviations

PEDOT:PSS	Poly(3,4-ethylenedioxythiophene)-poly(styrenesulfonate)
MPD	*m*-Phenylenediamine
TMC	Trimesoyl chloride
PANI	Polyaniline
CNT	Carbon nanotubes
GO	Graphene oxide
PVAm	Polyvinylamine
PDMS	Polydimethylsiloxane
MOF	Metal–organic framework
Pd	Palladium
sPPSU	Sulfonated polyphenylsulfone
PIM	Polymer of intrinsic microporosity
GG	Guar gum
Pt	Platinum
DI	De-ionized water
XPS	X-ray photoelectron spectroscopy
ESCA	Electron spectroscopy for chemical analysis
TEM	Transmission electron microscopy
FESEM	Field emission scanning electron microscopy
FTIR	Fourier transform infrared
C	Carbon
O	Oxygen
HRTEM	High-resolution transmission electron microscopy
SAED	Selected area electron diffraction
EDS	Energy-dispersive X-ray spectroscopy
P3HET	Poly(3-(2-hydroxyethyl)thiophene)
P3AcET	Poly(3-(2-acetoxyethyl)thiophene)
PPy	Polypyrrole
PEBA	Polyether block amide
EVA	Ethylene-vinyl acetate
PSF	Polysulfone
PVA	Polyvinyl alcohol
GOTMS	3-Glycidyloxypropyltrimethoxysilane
PEO-600	*O,O′*-bis (2-aminopropyl)polypropylene glycol-*block*-polyethylene
PEO-526	Poly(ethylene glycol) diglycidyl ether
MWCNT	Multi-walled carbon nanotube
TDI	2,4-Toluylene diisocyanate

Author contributions

All authors have contributed to the study's conception and design. Nishel Saini: sample preparation, data collection analysis, and writing – original draft. Gaurav Pandey: sample preparation and data analysis. Ankit Sharma: investigation and data analysis. Kamakshi Pandey: writing – review and editing.

Kamlendra Awasthi: supervision, conceptualization, and writing – review and editing.

Data availability

The data from this study can be made available on reasonable request.

Conflicts of interest

The authors declare that there is no conflict of interest that could influence the work reported in this paper.

Acknowledgements

References

1 M. Filonchyk, M. P. Peterson, L. Zhang, V. Hurynovich and Y. He, Greenhouse gases emissions and global climate change: Examining the influence of CO_2, CH_4, and N_2O, *Sci. Total Environ.*, 2024, 173359, DOI: **10.1016/J.SCITOTENV.2024.173359**.

2 R. M. Cigala, G. De Luca, I. Ielo and F. Crea, Biopolymeric Nanocomposites for CO_2 Capture, *Polymers*, 2024, **16**, 1063, DOI: **10.3390/POLYM16081063**.

3 H. T. Lu, W. Li, E. S. Miandoab, S. Kanehashi and G. Hu, The opportunity of membrane technology for hydrogen purification in the power to hydrogen (P2H) roadmap: a review, *Front. Chem. Sci. Eng.*, 2021, **15**, 464–482, DOI: **10.1007/s11705-020-1983-0**.

4 V. K. Kudapa, P. S. Paliyal, A. Mondal and S. Mondal, A Critical Review of Fabrication Strategies, Separation Techniques, Challenges, and Future Prospects for the Hydrogen Separation Membrane, *Fusion Sci. Technol.*, 2024, **80**, 803–825, DOI: **10.1080/15361055.2023.2290898**.

5 N. V. Blinova and F. Svec, Functionalized high performance polymer membranes for separation of carbon dioxide and methane, *J. Mater. Chem. A*, 2014, **2**, 600–604, DOI: **10.1039/c3ta14095d**.

6 J. Widakdo, H. F. M. Austria, T. M. Subrahmanya, E. Suharyadi, W. S. Hung, C. F. Wang, C. C. Hu, K. R. Lee and J. Y. Lai, Switching gas permeation through smart membranes by external stimuli: a review, *J. Mater. Chem. A*, 2022, **10**, 16743–16760, DOI: **10.1039/D2TA02756A**.

7 R. Kumar, Kamakshi, M. Kumar and K. Awasthi, Selective deposition of Pd nanoparticles in porous PET membrane for hydrogen separation, *Int. J. Hydrogen Energy*, 2017, **42**, 15203–15210, DOI: **10.1016/j.ijhydene.2017.03.202**.

8 N. Sazali, A comprehensive review of carbon molecular sieve membranes for hydrogen production and purification, *Int. J. Adv. Manuf. Technol.*, 2020, **107**, 2465–2483, DOI: **10.1007/s00170-020-05196-y**.

9 M. Wang, J. Zhao, X. Wang, A. Liu and K. K. Gleason, Recent progress on submicron gas-selective polymeric membranes, *J. Mater. Chem. A*, 2017, **5**, 8860–8886, DOI: **10.1039/c7ta01862b**.

10 Ankit, N. Saini, H. Pandey and K. Pandey, A Systematic Review of MOF, COF, and Their Hybrid-Based Composite Membranes for Gas Separation, *Macromol. Symp*, 2024, **413**, 2300058, DOI: **10.1002/MASY.202300058**.

11 Kamakshi, R. Kumar, V. K. Saraswat, M. Kumar and K. Awasthi, Active block copolymer layer on carboxyl-functionalized PET film for hydrogen separation, *Int. J. Hydrogen Energy*, 2020, **45**, 18676–18684, DOI: **10.1016/j.ijhydene.2019.07.174**.

12 M. M. Rahman, V. Filiz, S. Shishatskiy, C. Abetz, P. Georgopanos, M. M. Khan, S. Neumann and V. Abetz, Influence of Poly(ethylene glycol) Segment Length on CO_2 Permeation and Stability of PolyActive Membranes and Their Nanocomposites with PEG POSS, *ACS Appl. Mater. Interfaces*, 2015, **7**, 12289–12298, DOI: **10.1021/am504223f**.

13 N. Saini and K. Awasthi, Insights into the progress of polymeric nano-composite membranes for hydrogen separation and purification in the direction of sustainable energy resources, *Sep. Purif. Technol.*, 2022, **282**, 120029, DOI: **10.1016/J.SEPPUR.2021.120029**.

14 B. Hudaib, V. Gomes, J. Shi, C. Zhou and Z. Liu, Poly (vinylidene fluoride)/polyaniline/MWCNT nanocomposite ultrafiltration membrane for natural organic matter removal, *Sep. Purif. Technol.*, 2018, **190**, 143–155, DOI: **10.1016/j.seppur.2017.08.026**.

15 Z. Ali, F. Pacheco, E. Litwiller, Y. Wang, Y. Han and I. Pinnau, Ultra-selective defect-free interfacially polymerized molecular sieve thin-film composite membranes for H_2 purification, *J. Mater. Chem. A*, 2018, **6**, 30–35, DOI: **10.1039/c7ta07819f**.

16 Y. Wang, L. Li, X. Zhang, J. Li, C. Liu, N. Li and Z. Xie, Polyvinylamine/graphene oxide/PANI@CNTs mixed matrix composite membranes with enhanced CO_2/N_2 separation performance, *J. Membr. Sci.*, 2019, **589**, 117246, DOI: **10.1016/j.memsci.2019.117246**.

17 F. U. Nigiz and N. D. Hilmioglu, Enhanced hydrogen purification by graphene - Poly(Dimethyl siloxane) membrane, *Int. J. Hydrogen Energy*, 2020, **45**, 3549–3557, DOI: **10.1016/j.ijhydene.2018.12.215**.

18 G. Dong, H. Li and V. Chen, Challenges and opportunities for mixed-matrix membranes for gas separation, *J. Mater. Chem. A*, 2013, **1**, 4610–4630, DOI: **10.1039/C3TA00927K**.

19 L. Zhu, M. T. Swihart and H. Lin, Tightening polybenzimidazole (PBI) nanostructure via chemical cross-linking for membrane H_2/CO_2 separation, *J. Mater. Chem. A*, 2017, **5**, 19914–19923, DOI: **10.1039/c7ta03874g**.

20 Q. Xin, Y. Pan, C. Zhang, L. Zhang, C. Dong, L. Lin, L. Zhao, H. Ye and Y. Zhang, An exploration of novel

natural gas leak detection based on the efficient CH_4/N_2 separation of polymer blend membrane, *Sep. Purif. Technol.*, 2024, **336**, 126302, DOI: **10.1016/J. SEPPUR.2024.126302**.

21 A. Samir, F. H. Ashour, A. A. A. Hakim and M. Bassyouni, Recent advances in biodegradable polymers for sustainable applications, *Mater. Degrad.*, 2022, **6**, 1–28, DOI: **10.1038/ s41529-022-00277-7**.

22 A. Msahel, F. Galiano, M. Pilloni, F. Russo, A. Hafiane, R. Castro-Muñoz, V. B. Kumar, A. Gedanken, G. Ennas, Z. Porat, A. Scano, S. Ben Hamouda and A. Figoli, Exploring the Effect of Iron Metal-Organic Framework Particles in Polylactic Acid Membranes for the Azeotropic Separation of Organic/Organic Mixtures by Pervaporation, *Membranes*, 2021, **11**, 65, DOI: **10.3390/MEMBRANES11010065**.

23 N. Pal and M. Agarwal, Efficient performance of natural polysaccharide-based mixed matrix membrane for CO_2/H_2 and CO_2/N_2 mixed gas separation, *Int. J. Hydrogen Energy*, 2024, **57**, 273–289, DOI: **10.1016/J.IJHYDENE.2024.01.019**.

24 N. Pal, N. Saini, M. Agarwal and K. Awasthi, Experimental investigation of natural polysaccharide-based mixed matrix membrane modified with graphene oxide and Pd-nanoparticles for enhanced gas separation performance, *Int. J. Hydrogen Energy*, 2022, **47**, 41820–41832, DOI: **10.1016/J.IJHYDENE.2022.03.049**.

25 A. Saha, Polymer Nanocomposites: A Review on Recent Advances in the Field of Green Polymer Nanocomposites, *Curr. Nanosci.*, 2023, **20**, 706–716, DOI: **10.2174/ 0115734137274950231113050300**.

26 G. Satchanska, S. Davidova and P. D. Petrov, Natural and Synthetic Polymers for Biomedical and Environmental Applications, *Polymers*, 2024, **16**, 1159, DOI: **10.3390/ POLYM16081159**.

27 A. Ito, T. Yasuda, T. Yoshioka, A. Yoshida, X. Li, K. Hashimoto, K. Nagai, M. Shibayama and M. Watanabe, Sulfonated Polyimide/Ionic Liquid Composite Membranes for CO_2 Separation: Transport Properties in Relation to Their Nanostructures, *Macromolecules*, 2018, **51**, 7112–7120, DOI: **10.1021/acs.macromol.8b01135**.

28 W. F. Yong, Z. K. Lee, T. Chung, M. Weber, S. Claudia and C. Maletzko, Blends of a Polymer of Intrinsic Microporosity and Partially Sulfonated Polyphenylenesulfone for Gas Separation, *ChemSusChem*, 2016, **9**, 1953–1962, DOI: **10.1002/CSSC.201600354**.

29 W. Lu, D. Yuan, J. Sculley, D. Zhao, R. Krishna and H. C. Zhou, Sulfonate-grafted porous polymer networks for preferential CO_2 adsorption at low pressure, *J. Am. Chem. Soc.*, 2011, **133**, 18126–18129, DOI: **10.1021/ja2087773**.

30 M.-H. Yoon, Y. Kim and J. Kim, Conductive polymer microfiber mesh structure, manufacturing method thereof and electrode for flexible electronic device using the same, US20220020509A1, 2021. **https://patents.google.com/ patent/US20220020509A1/en** (accessed September 28, 2023).

31 S. M. Kim, C. H. Kim, Y. Kim, N. Kim, W. J. Lee, E. H. Lee, D. Kim, S. Park, K. Lee, J. Rivnay and M. H. Yoon,

32 J. Wang, X. Lv, L. Huang, L. Li, X. Li and J. Zhang, Construction of amphiphilic networks in blend membranes for CO_2 separation, *Korean J. Chem. Eng.*, 2023, **40**, 175–184, DOI: **10.1007/S11814-022-1236-7/METRICS**.

33 N. Saini, D. Y. Lee, M. H. Yoon and K. Awasthi, Unveiling the Potential of Pt Nanoparticle-Decorated PEDOT:PSS Membranes for Efficient Gas Separation, *ACS Appl. Mater. Interfaces*, 2024, **16**, 7700–7708, DOI: **10.1021/ acsami.3c15763**.

34 N. Saini, S. Agarwal and K. Awasthi, Bimetallic PdPt alloy nanoparticle-decorated track-etched polyethylene terephthalate membranes for efficient H_2 separation, *Mater. Adv.*, 2024, **5**, 2906–2916, DOI: **10.1039/D3MA00896G**.

35 R. Kumar, Kamakshi, M. Kumar and K. Awasthi, Functionalized Pd-decorated and aligned MWCNTs in polycarbonate as a selective membrane for hydrogen separation, *Int. J. Hydrogen Energy*, 2016, **41**, 23057–23066, DOI: **10.1016/j.ijhydene.2016.09.008**.

36 J. Golubović, L. Rakočević, D. Vasiljević Radović and S. Štrbac, Improved Oxygen Reduction on GC-Supported Large-Sized Pt Nanoparticles by the Addition of Pd, *Catalysts*, 2022, **12**, 968, DOI: **10.3390/CATAL12090968**.

37 C. A. Rodríguez-Proenza, J. P. Palomares-Báez, M. A. Chávez-Rojo, A. F. García-Ruiz, C. L. Azanza-Ricardo, A. Santoveña-Uribe, G. Luna-Bárcenas, J. L. Rodríguez-López and R. Esparza, *Atomic Surface Segregation and Structural Characterization of PdPt Bimetallic Nanoparticles, Mater*, Basel, Switzerland, 2018, vol. 11. DOI: **10.3390/ MA11101882**.

38 A. G. Shard, Practical guides for X-ray photoelectron spectroscopy: Quantitative XPS, *J. Vac. Sci. Technol., A*, 2020, **38**, 041201, DOI: **10.1116/1.5141395**.

39 O. Rosseler, C. Ulhaq-Bouillet, A. Bonnefont, S. Pronkin, E. Savinova, A. Louvet, V. Keller and N. Keller, Structural and electronic effects in bimetallic PdPt nanoparticles on TiO_2 for improved photocatalytic oxidation of CO in the presence of humidity, *Appl. Catal., B*, 2015, **166–167**, 381–392, DOI: **10.1016/j.apcatb.2014.12.001**.

40 A. Aygun, F. Gulbagca, E. E. Altuner, M. Bekmezci, T. Gur, H. Karimi-Maleh, F. Karimi, Y. Vasseghian and F. Sen, Highly active PdPt bimetallic nanoparticles synthesized by one-step bioreduction method: Characterizations, anticancer, antibacterial activities and evaluation of their catalytic effect for hydrogen generation, *Int. J. Hydrogen Energy*, 2023, **48**, 6666–6679, DOI: **10.1016/J.IJHYDENE.2021.12.144**.

41 F.-M. Li, X.-Q. Gao, S.-N. Li, Y. Chen and J.-M. Lee, Thermal decomposition synthesis of functionalized PdPt alloy nanodendrites with high selectivity for oxygen reduction reaction, *NPG Asia Mater.*, 2015, **7**, e219–e219, DOI: **10.1038/ am.2015.108**.

42 X. Meng, M. Bi and W. Gao, Shape and composition effects of PdPt bimetallic nanocrystals on hydrogen sensing pro-

perties of SnO$_2$ based sensors, *Sens. Actuators, B*, 2023, **390**, 133976, DOI: **10.1016/j.snb.2023.133976**.

43 K. Dutta, B. Das, D. Mondal, A. Adhikari, D. Rana, A. Kumar Chattopadhyay, R. Banerjee, R. Mishra and D. Chattopadhyay, An ex situ approach to fabricating nano-silica reinforced polyacrylamide grafted guar gum nano-composites as an efficient biomaterial for transdermal drug delivery application, *New J. Chem.*, 2017, **41**, 9461–9471, DOI: **10.1039/C7NJ01713H**.

44 Q. Zhao, R. Jamal, L. Zhang, M. Wang and T. Abdiryim, The structure and properties of PEDOT synthesized by tem-plate-free solution method, *Nanoscale Res. Lett.*, 2014, **9**, 557, DOI: **10.1186/1556-276X-9-557/FIGURES/9**.

45 Y. Liu, D. Sun, S. Askari, J. Patel, M. Macias-Montero, S. Mitra, R. Zhang, W. F. Lin, D. Mariotti and P. Maguire, Enhanced Dispersion of TiO$_2$ Nanoparticles in a TiO2/PEDOT:PSS Hybrid Nanocomposite via Plasma-Liquid Interactions, *Sci. Rep.*, 2015, **51**(5), 1–11, DOI: **10.1038/srep15765**.

46 J. H. Lee, J. P. Jung, E. Jang, K. B. Lee, Y. J. Hwang, B. K. Min and J. H. Kim, PEDOT-PSS embedded comb copolymer membranes with improved CO$_2$ capture, *J. Membr. Sci.*, 2016, **518**, 21–30, DOI: **10.1016/J.MEMSCI.2016.06.025**.

47 I. Del Agua, D. Mantione, N. Casado, A. Sanchez-Sanchez, G. G. Malliaras and D. Mecerreyes, Conducting Polymer Iongels Based on PEDOT and Guar Gum, *ACS Macro Lett.*, 2017, **6**, 473–478, DOI: **10.1021/acsmacrolett.7b00104**.

48 L. Guo, H. Sato, T. Hashimoto and Y. Ozaki, FTIR Study on Hydrogen-Bonding Interactions in Biodegradable Polymer Blends of Poly(3-hydroxybutyrate) and Poly(4-vinylphenol), *Macromolecules*, 2010, **43**, 3897–3902, DOI: **10.1021/ma100307m**.

49 J.-Y. Ye, Y.-X. Jiang, T. Sheng and S.-G. Sun, *In situ* FTIR spectroscopic studies of electrocatalytic reactions and pro-cesses, *Nano Energy*, 2016, **29**, 414–427, DOI: **10.1016/j.nanoen.2016.06.023**.

50 S. Nešpůrek, P. Kuberský, R. Polanský, M. Trchová, J. Šebera and V. Sychrovský, Raman spectroscopy and DFT calculations of PEDOT:PSS in a dipolar field, *Phys. Chem. Chem. Phys.*, 2021, **24**, 541–550, DOI: **10.1039/D1CP03899K**.

51 R. Anitha, S. S. Menon, G. Bhalerao, P. Siddham, K. Baskar and S. Singh, Electrical properties of nitric acid and DMSO treated PEDOT:PSS/n-Si hybrid heterostructures for opto-electronic applications, *J. Appl. Polym. Sci.*, 2020, **137**, 48952, DOI: **10.1002/APP.48952**.

52 G. Palumbo, K. Berent, E. Proniewicz and J. Banaś, Guar Gum as an Eco-Friendly Corrosion Inhibitor for Pure Aluminium in 1-M HCl Solution, *Materials*, 2019, **12**, 2620, DOI: **10.3390/MA12162620**.

53 M. Szymańska-Chargot, M. Chylińska, P. M. Pieczywek, P. Rösch, M. Schmitt, J. Popp and A. Zdunek, Raman imaging of changes in the polysaccharides distribution in the cell wall during apple fruit development and senes-cence, *Planta*, 2016, **243**, 945, DOI: **10.1007/S00425-015-2456-4**.

54 M. Kong, M. Garriga, J. S. Reparaz and M. I. Alonso, Advanced Optical Characterization of PEDOT:PSS by Combining Spectroscopic Ellipsometry and Raman Scattering, *ACS Omega*, 2022, **7**, 39429–39436, DOI: **10.1021/acsomega.2c05945**.

55 Y. Wang, S. Wu, Q. Yin, B. Jiang and S. Mo, Tuning thermo-electric performance of Poly(3,4-ethylenedioxythiophene): Poly (styrene sulfonate)/Polyaniline composite films by nanostructure evolution of polyaniline, *Polym. Test.*, 2021, **94**, 107017, DOI: **10.1016/J.POLYMERTESTING.2020.107017**.

56 M. Farnam, H. Mukhtar and A. M. Shariff, An investigation of blended polymeric membranes and their gas separation performance, *RSC Adv.*, 2016, **6**, 102671–102679, DOI: **10.1039/C6RA21574B**.

57 Y. Li, Y. Pang, L. Wang, Q. Li, B. Liu, J. Li, S. Liu and Q. Zhao, Boosting the Performance of PEDOT:PSS Based Electronics Via Ionic Liquids, *Adv. Mater.*, 2024, **36**, 2310973, DOI: **10.1002/ADMA.202310973**.

58 H. Warren and M. Panhuis, Electrically conducting PEDOT: PSS - Gellan Gum Hydrogels, *Mater. Res. Soc. Symp. Proc.*, 2013, **1569**, 219–223, DOI: **10.1557/OPL.2013.1101**.

59 B. D. Reid, V. H. M. Ebron, I. H. Musselman, J. P. Ferraris and K. J. Balkus, Enhanced gas selectivity in thin film com-posite membranes of poly(3-(2-acetoxyethyl)thiophene), *J. Membr. Sci.*, 2002, **195**, 181–192, DOI: **10.1016/S0376-7388(01)00551-8**.

60 X. Wang, X. Ding, H. Zhao, J. Fu, Q. Xin and Y. Zhang, Pebax-based mixed matrix membranes containing hollow polypyrrole nanospheres with mesoporous shells for enhanced gas permeation performance, *J. Membr. Sci.*, 2020, **602**, 117968, DOI: **10.1016/J.MEMSCI.2020.117968**.

61 P. Hacarlioglu, L. Toppare and L. Yilmaz, Polycarbonate – polypyrrole mixed matrix gas separation membranes, *J. Membr. Sci.*, 2003, **225**, 51–62, DOI: **10.1016/S0376-7388(03)00342-9**.

62 N. Y. Huang, C. C. Wang and C. Y. Chen, Gas-permeation properties of sandwich-like polyaniline/poly(ethylene vinyl acetate) nanocomposite membranes, *Chem. Eng. Res. Des.*, 2021, **170**, 239–247, DOI: **10.1016/J.CHERD.2021.03.020**.

63 H. J. Lee and S. W. Kang, CO2 Separation with Polymer/Aniline Composite Membranes, *Polymers*, 2020, **12**, 1363, DOI: **10.3390/polym12061363**.

64 T. Ito, R. Shiota, N. Taniguchi, R. J. Spontak and K. Nagai, Gas-separation and physical properties of ABA triblock copolymers synthesized from polyimide and hydrophilic adamantane derivatives, *Polymer*, 2020, **202**, 122642, DOI: **10.1016/j.polymer.2020.122642**.

65 W. Xiao, P. Gao, Y. Dai, X. Ruan, X. Jiang, X. Wu, Y. Fang and G. He, Efficiency separation process of H$_2$/CO$_2$/CH$_4$ mixtures by a hollow fiber dual membrane separator, *Processes*, 2020, **8**, 560, DOI: **10.3390/PR8050560**.

66 L. Shao and T. S. Chung, In situ fabrication of cross-linked PEO/silica reverse-selective membranes for hydrogen purifi-cation, *Int. J. Hydrogen Energy*, 2009, **34**, 6492–6504, DOI: **10.1016/j.ijhydene.2009.05.137**.

67 L. Shao, S. Quan, X. Q. Cheng, X. J. Chang, H. G. Sun and R. G. Wang, Developing cross-linked poly(ethylene oxide) membrane by the novel reaction system for H2 purification, *Int. J. Hydrogen Energy*, 2013, **38**, 5122–5132, DOI: **10.1016/j.ijhydene.2013.02.050**.

68 R. S. Murali, S. Sridhar, T. Sankarshana and Y. V. L. Ravikumar, Gas Permeation Behavior of Pebax-1657 Nanocomposite Membrane Incorporated with Multiwalled Carbon Nanotubes, *Ind. Eng. Chem. Res.*, 2010, **49**, 6530–6538, DOI: **10.1021/IE9016495**.

69 X. Wu, W. Liu, H. Wu, X. Zong, L. Yang, Y. Wu, Y. Ren, C. Shi, S. Wang and Z. Jiang, Nanoporous ZIF-67 embedded polymers of intrinsic microporosity membranes with enhanced gas separation performance, *J. Membr. Sci.*, 2018, **548**, 309–318, DOI: **10.1016/J.MEMSCI.2017.11.038**.

This journal is © The Royal Society of Chemistry 2025